PAPER

Experimental study on plasma generated by a tapered coaxial accelerator and its damage effects on a tungsten target at different angles

IOP Publishing Plasma Physics and Controlled Fusion
Plasma Phys. Control. Fusion **65** (2023) 015012 (14pp) https://doi.org/10.1088/1361-6587/aca4f6

Experimental study on plasma generated by a tapered coaxial accelerator and its damage effects on a tungsten target at different angles

Chongxiao Zhao[1,2,*], YiYi Chen[1,3], Jian Song[2], Xianxiu Mei[2], Qikun Pan[1], RanRan Zhang[1], Liang Yang[4], Fantao Zhao[2], Jiawen Li[2] and Dezhen Wang[2]

[1] State Key Laboratory of Laser Interaction with Matter, Changchun Institute of Optics, Fine Mechanics and Physics, Chinese Academy of Sciences, Changchun 130033, People's Republic of China
[2] Key Laboratory of Materials Modification by Laser, Ion, and Electron Beams of the Ministry of Education, School of Physics, Dalian University of Technology, Dalian 116024, People's Republic of China
[3] University of Chinese Academy of Sciences, Beijing 100049, People's Republic of China
[4] Key Laboratory of Chemical lasers, Chinese Academy of Science, Dalian Institute of Chemical Physics, Dalian 116023, People's Republic of China

E-mail: zhaochognxiao@ciomp.ac.cn

Received 24 June 2022, revised 8 November 2022
Accepted for publication 22 November 2022
Published 8 December 2022

Abstract

Plasma wall interaction inevitably occurs during the operation of tokamaks. The coaxial gun device has low operation cost and the parameters of plasma produced by the gun are close to those of type I edge localized mode (ELM); therefore, the coaxial gun is suitable in simulation experiments as a heat flux source of transient events such as type I ELM under the condition of H-mode in the International Thermonuclear Experimental Reactor. In this paper, the plasma generated by the discharge of a tapered coaxial accelerator thermal shock on a tungsten target is used to simulate the damage effect of the divertor. The plasma parameters are measured in the experiment. The velocity of the plasma is 41.7 km s^{-1}, and the kinetic energy of a single hydrogen ion is 9.2 eV. The energy density at the center of the plasma can reach 1.5 MJ m^{-2}, and the density can reach about 2.78 $\times$ 10^{15} cm^{-3}. The reflection of plasma in the process of exposure at different angles is observed. It is observed that droplets of millimeter size splash from the target. Traces of liquid flow are observed on the surface of the target, which shows that there is a melting process on the surface of the target. The mass loss of the target is of the order of milligrams after 20 pulses. The ablation and residual stress of the target surface both decrease with a decrease in the angle. This is because the accumulated energy per unit area of the target surface decreases with a decrease in the angle. The results of the simulation experiment help us to understand the working state around the divertor target in tokamak devices.

* Author to whom any correspondence should be addressed.

Supplementary material for this article is available online

Keywords: tapered coaxial gun, discharge mode, plasma parameter diagnosis, tungsten materials thermal shock damage

(Some figures may appear in colour only in the online journal)

1. Introduction

A large number of studies have been carried out on the plasma surface interaction (PSI) of divertors during H-mode plasma operation with type I ELMs [1–6], including experimental simulation and theoretical calculation. The heat loads during the International Thermonuclear Experimental Reactor (ITER) ELMs-I are estimated to be $Q_{\mathrm{ELM}} = (1\text{–}3)$ MJ m^{-2}, with a pulse length of 0.1–1 ms [1, 4, 6, 7]. The high energy may cause the breakdown and melting of the divertor W target and movement of the melting layer, etc, resulting in shortening the lifetime of the divertors. Due to the high energy density, temperature and density, the plasma produced by a coaxial gun discharge can simulate the thermal shock effect of PSI and the effect of particle flow [8, 9].

Many research groups have used a coaxial gun to simulate the damage effect of ELM-I on the divertor wall material in tokamaks. The National Science Center Kharkov Institute of Physics and Technology (NSC-KIPT) not only studied the characteristics of plasma and PSI but also studied the characterization of the materials in detail using a self-developed piece of equipment called a quasi-stationary plasma accelerator (QSPA) [1, 10]. NSC-KIPT also did other research on ITER with QSPA/QSPA-M. The Graduate School of Engineering at Hyogo University in Japan has carried out research related to a compact toroidal plasma with an external magnetic field and surface damage characteristics of material for ITER [3, 4, 6]. The Troitsk Institute for Innovation and Fusion Research has studied plasma/material interaction in disruption simulation experiments at the plasma gun facility MK-200 UG [7, 11].

With the development of ITER, the heat load of ELMs increases gradually, so it is necessary to use a higher parameter plasma source for simulation experiments. In order to get more suitable results for tokamak in the simulation experiments using a coaxial plasma gun, a tapered coaxial gun with negative pulse was used [12]. Previous studies have shown that the energy density and electron energy of the plasma ejected from the muzzle of a tapered coaxial gun are higher than those of a cylindrical gun because of the physical compression [13]. On the other hand, the plasmoid ejected from a tapered gun is relatively uniform and can maintain collimation [12].

In the current tokamak operating state, the angle between the plasma transport direction and the vertical direction of the divertor target is variable. The damage effect of the varying angles on the target is different [14]. NSC-KIPT have used a variety of measuring instruments to observe the bombardment process at different angles and different pulses by QSPA/QSPA-M [10, 15]. Material characterization is carried out for the target after plasma bombardment at different angles in this study. The blow-by phenomenon occurs in the discharge process of a cylindrical coaxial gun [9, 13, 16–18]. Based on previous research, the blow-by results in tilt of the plasma sheet and inhomogeneous distribution of the plasma in the coaxial gun. Therefore, a conventional cylindrical coaxial gun needs to be further optimized as a plasma source for the simulation experiments.

Tungsten is selected as the plasma-facing material for most ITER divertors and DEMO first walls because of its properties [5, 6, 10, 19]. In the process of plasma thermal shock on a tungsten target, the tungsten surface is ablated and melted, causing droplet splashing and so on. In addition, the thermal shock causes a change in residual stress on the surface of the tungsten target. These phenomena need to be analyzed in depth. In this paper, the tungsten targets are subjected to 20 thermal shock pulses by the gun. The target is rotated to different angles from the plasma transport direction during the thermal shock to study the damage effect.

In tokamak devices, the divertor flows contain primarily hydrogen isotopes. In order to simulate the working environment of divertors more realistically, hydrogen is selected as the working gas. Combined with the above, in this paper, the development of the experimental platform is introduced. The plasma parameters produced by a tapered gun are measured. In addition, the process of plasma thermal shock on the surface of the tungsten target is observed. The damage effect on the target surface after 20 pulses in different angles is studied. The remainder of this paper is organized as follows: section 2 gives an overview of the experimental setup and diagnostics. Section 3 presents the experimental results and discussion, mainly divided into characteristics of plasma, interaction between the plasma and target, and material characterization. A summary is reported in section 4.

2. Experimental setup

A schematic of the experimental equipment is shown in figure 1(a). The tapered coaxial gun is composed of a tapered copper central cathode and a coaxial stainless outer anode. The outer diameter of the inner electrode is 70 mm and the inner diameter of the outer electrode is 90 mm at the bottom. The spacing between the inner and outer electrodes is equal at each position. The power supply consists of six capacitors of 25 μF in parallel, with a total capacitance of 150 μF. This paper analyzes the characteristics of plasma and the

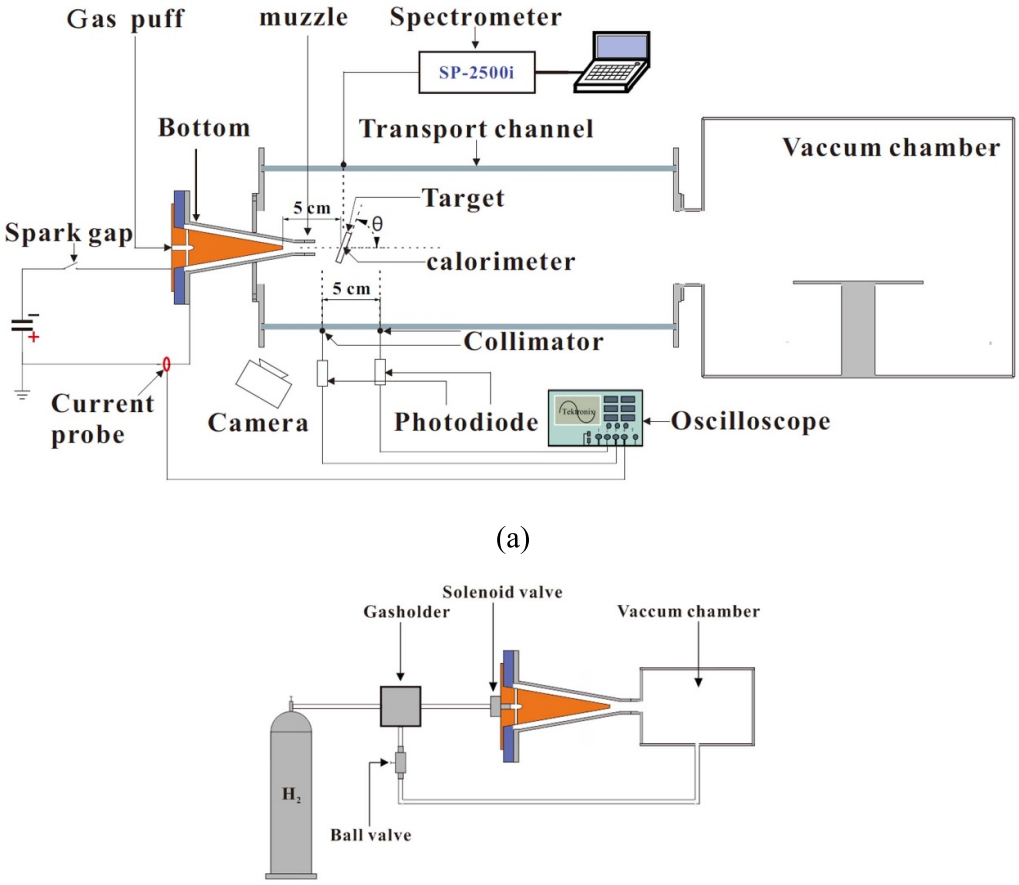

Figure 1. Schematic of (a) experimental devices and (b) gas path.

damage effect of plasma thermal shock on tungsten target at 16 kV of the charging voltage and 20 pulses of the discharge time. The pulse period is 1 min. The transport channel of the plasma is composed of a toughened glass cylinder, in order to observe the experimental phenomenon clearly. The inner diameter and length of the toughened glass cylinder are 400 mm and 800 mm, respectively. In order to get more suitable results for tokamak in the simulation, the pressure in the vacuum chamber is pumped to a minimum (10^{-4} Pa), and the working gas used in the experiment is hydrogen. The gas flow path is shown in figure 1(b). When the vacuum chamber is pumped to 10^{-4} Pa, the ball valve is closed and the hydrogen cylinder is opened. The mass and time of the gas are controlled by a solenoid valve. The discharge mode is pre-filled mode: when the gas flows through the solenoid valve and fills the gun, the bottom of the tapered gun breaks down and plasma is generated.

Tungsten with a purity over of 99.95%, provided by Xiamen Honglu Tungsten Molybdenum Industry Co., Ltd as a target with a square cross-section of 30 × 30 mm^2, is used in this study. The thickness of the cut target is 2 mm. In the experiment, the distance between the center of the target and the inner electrode of the tapered gun is 5 cm. The surface of the target is kept at room temperature before exposure.

The measuring equipment of the plasma parameters includes a spectrometer (SP-2500i), an oscilloscope (PicoScope 4000 Series), a Pearson current probe, photodiodes (THORLABS PDA10A-EC), and optical fiber collimators (THORLABS F240SMA-A); the full angle beam divergence of the collimators is 0.027°. The collimators connected to the photodiodes by optical fibers are placed at the muzzle of the gun, and the distance between the two collimators is 5 cm. The specific positions of the collimators are shown in figure 1(a). By obtaining the time of the first peak of the optical signal and the specific position of the two collimators, the velocity can be calculated. If the distance between the two collimators is too small, the calculated velocity causes error; if the distance between two collimators is too large, the calculated velocity cannot represent the average velocity. The full spectrum of the plasma is measured by a spectrometer, and the impurity in the plasma can be observed by analyzing the spectrum line. The plasma density is calculated using the Stark broadening method. The radial distribution of the plasma energy density at the target location is obtained using a calorimeter. The calorimeter is made of a thermistor, with the model being Pt100 and an accuracy of up to 0.1 K. The calorimeter is placed at distances of 0, 5 and 10 mm from the center axis of the gun. The measuring diameter of the calorimeter is 5 mm.

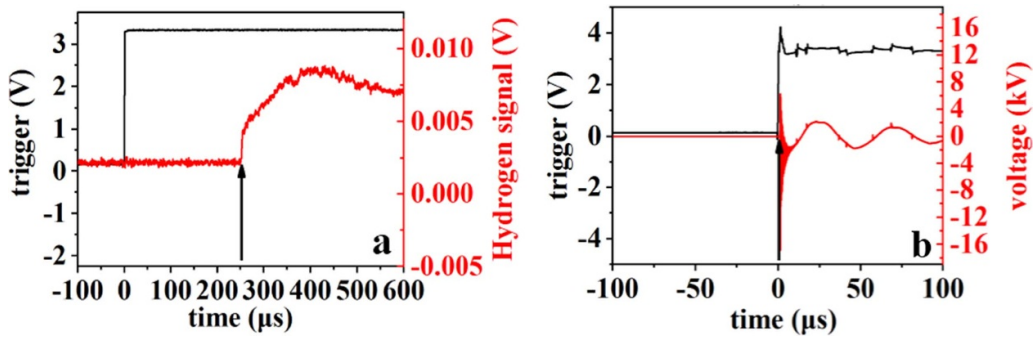

Figure 2. (a) Interval between the time of hydrogen reaching the muzzle and the trigger signal and (b) interval between the time of gas breakdown at the breech of the tapered coaxial gun and the trigger signal.

A high-speed camera (Veo 410L) is used to photograph the process of plasma thermal shocks on the targets at different angles. In order to observe the ablation of the tungsten surface and the cracks with micrometer widths that appear on the surface of the target, a metalloscope (OLYMPUS GX51) and a scanning electron microscope (SEM) are used in the experiment. The thermal shock of the plasma affects the surface characteristics of the target. In order to analyze the damage effect further, an x-ray diffraction meter (XRD) is used to diagnose the target surface.

The discharge mode of the gun in this experiment is prefilled mode [20–23]. The pressure sensor (PCB 113B21) is used to measure the air pressure signal at the muzzle position, and the current probe is used to measure the current signal in the discharge process. As can be seen from figures 2 (a) and (b), the interval between the time the hydrogen reaches the muzzle and the trigger signal is 250 μs, and the interval between the time of gas breakdown at the breech of the tapered coaxial gun and the trigger signal is 1 μs. The mass of hydrogen through the valve is 1.56 mg per pulse, and the duration of hydrogen supply is 1.22×10^{-3} s. The calculated hydrogen particle flux is 1.23×10^{27} s^{-1} m^{2}.

3. Results and discussion

3.1. Characteristics of plasma

The charging voltage of the capacitor is 16 kV. When the gas reaches the muzzle, hydrogen is broken down from the bottom of the gun. The plasma is ejected from the muzzle by Lorentz force and thermal expansion.

Figure 3 shows the current signal in the discharge process and the optical signals measured by two photodiodes. The single cycle of the loop current is about 20 μs. The current waveform is a gradually decaying sine wave, indicating that there are always one or more current paths in the coaxial gun during the discharge process. The peak current of the first half cycle is 270 kA. The time interval between the two optical signals is $\triangle t = 1.2$ μs. The transport velocity v of the plasma is 41.7 km s^{-1} by the formula $v = L/\triangle t$. If the velocity of the plasma head is higher than the tail, the calculated value is maximum. The single ion kinetic energy of hydrogen is

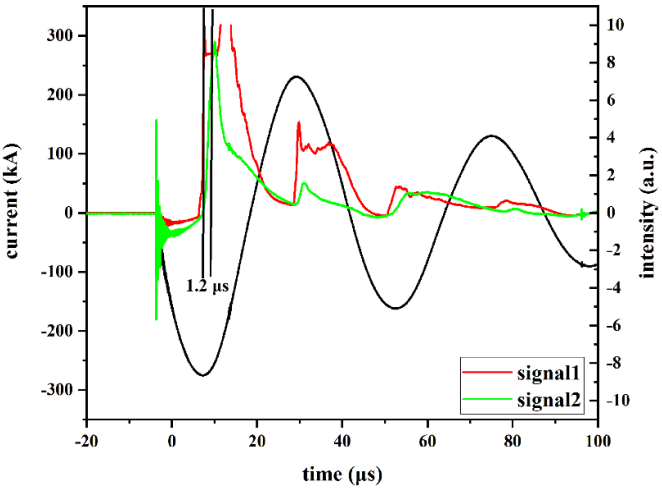

Figure 3. Discharge current and photocurrent signals at a charging voltage of 16 kV and hydrogen particle flux of 1.23×10^{27} s^{-1} m^{2}.

9.2 eV at this condition using the kinetic energy theorem formula $E = (1/2)mv^2$.

As shown in figure 4(a), the radial energy density distribution of the plasma at the target location is obtained by a calorimeter. The energy density at the center of the plasmoid is about 1.5 MJ m^{-2}. The energy density of the plasmoid decreases from the center to the edge. In the process of plasma transport in the vacuum chamber, the thermal diffusion makes the energy density decrease from the center to the edge. The energy density at the edge of the plasmoid is 1.1 MJ m^{-2}. As can be seen from the photocurrent signal in figure 3, the duration of the plasma stream $\triangle t_{\rm p}$ is 50 μs, it can be estimated that the average power density at the center of the plasma is about 30 GW m^{-2}, and that at the edge is about 22 GW m^{-2}. Figure 4(b) shows the radial average power density distribution of plasma at the target location.

The researchers in [23] mentioned that the temperature increase $\triangle T_{tr}$ at the surface of the tested material is a major characteristic of the transient heat load. The temperature increase in pulse duration $\triangle t_p$ can be expressed as [24]:

$$VT_{tr} = 2L\sqrt{\frac{Vt}{\pi\lambda Qc_p}} \tag{1}$$

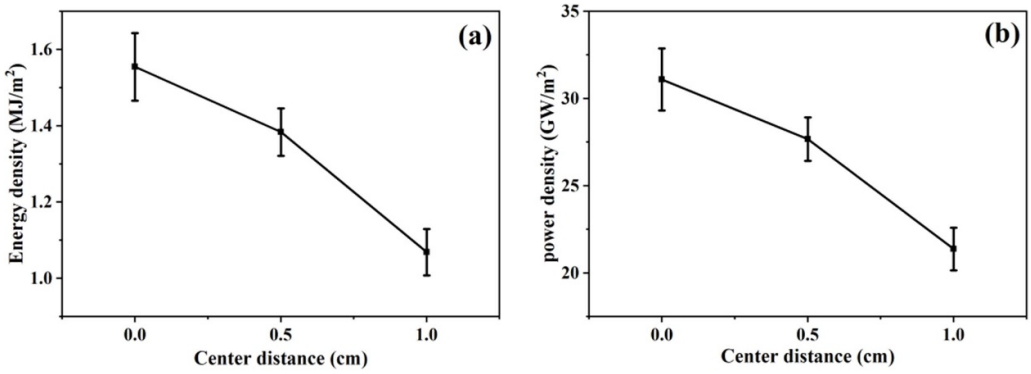

Figure 4. (a) Energy density and (b) power density at the target location varying with the center distance.

where L is the constant power density, λ is the thermal conductivity, Q is the density and the c_p is the specific. The heat flux factor (also called the heat flux parameter or damage factor) is expressed as:

$$F_{\mathrm{HF}} = L\sqrt{\Delta t}. \tag{2}$$

The heat flux factor which is proportional to $\triangle T_{tr}$ is derived from this equation to compare experiments with different pulse durations and power densities. The calculated heat flux factor at the center of the plasma is 212.1 $\mathrm{MWs}^{1/2}$ m^{-2}.

As shown in figure 5 from the full spectrum, there are not only H_α, H_β and H_γ lines, but also copper ion lines. The intensity of copper ions in the spectral line is the weakest, indicating that there is a small amount of copper impurities in the plasma. These small amounts of copper impurities are mainly caused by the ion bombardment of the cathode during the discharge. The copper impurities are mixed into the hydrogen plasma and ejected from the muzzle of the gun. In later experiments, the electrode can be coated with tungsten in the design of the coaxial gun to further avoid the problem of impurities caused by ablating the electrode.

In this paper, the Stark broadening method is used to calculate the electron density [9, 12, 23, 25–28]. The fitted line as shown in figure 6(a) can be obtained by fitting the H_β line in figure 5. This paper enumerates the parameters for density calculation. The specific method of Stark broadening calculation has been described in detail in other articles of the author [12, 28]. The value obtained at this position is the largest density of plasma. The spectrum line broadening of the fitting obtained H_β line is 1.388 mm (full width at half maximum). Figure 6(b) shows the instrument broadening measured by a He–Ne laser and the fitted line. The spectrum line broadening of the fitting line of the He–Ne laser is 0.465 nm. The electron density n_e obtained under the above discharge parameters is about 2.78×10^{15} cm^{-3}; the calculated value is the maximum. The calculated plasma flux to the target is 1.16×10^{26} s^{-1} m^2 by the formula $\gamma = n_\mathrm{e} \cdot v$. In summary, the essential data of the tapered accelerator are shown in table 1.

Table 2 shows the essential data of QSPA kh-50 from the official website of NSC-KIPT, and table 3 shows the key design parameters and type I ELM characteristic parameters

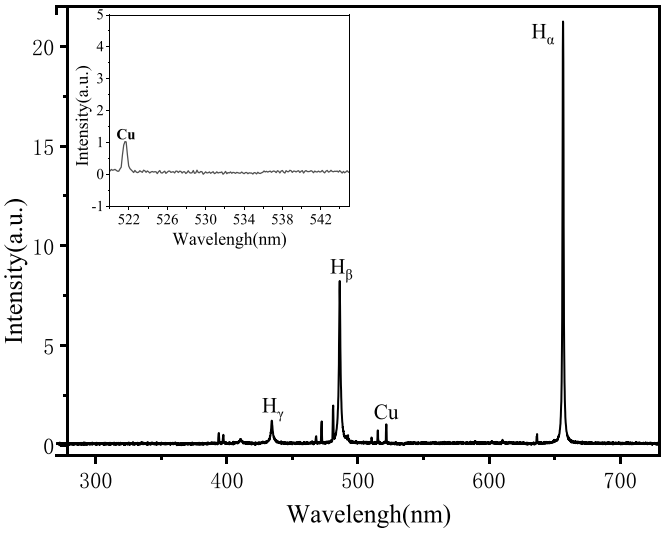

Figure 5. Full spectrum of the plasma at the target location at a charging voltage of 16 kV and gas mass of 1.56 mg.

assumed in the analysis obtained from [29]. Through the analysis of tables 1–3, we find that the energy density and electron density of plasma produced by the tapered gun basically conform to the parameters of ELM. The duration of the tapered gun is relatively short. The average power density of the tapered gun is much higher than that of type I ELM. The heat flux factor of the tapered gun is relatively high.

These results are mainly due to the short current cycle and short electrode length of the actual tapered gun. Therefore, in order to make the plasma parameters more consistent with the nuclear fusion device for simulation experiments, the research group plans to further optimize the power supply parameters, circuit design and electrode structure on the basis of the existing conical gun discharge accelerator. At present, the research group has built a pulse power supply with a maximum frequency of 50 Hz. In addition, referring to the real situation in ITER devices, the research group is also considering applying an external magnetic field to the target that conforms to the simulation experiment.

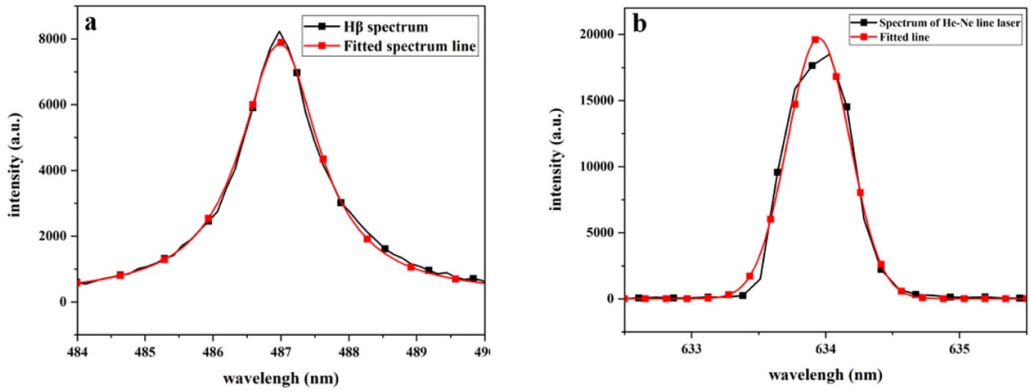

Figure 6. (a) H_β spectral line and its fitting spectral line; the broadening of this spectrum is 1.388 nm. (b) Instrument broadening measured using a He–Ne laser; spectrum broadening is 0.465 nm.

Table 1. Essential parameters of the tapered accelerator.

Charging voltage	16 kV
Peak current	270 kA
Particle flux	1.23×10^{27} s^{-1} m^2
Duration	50 μs
Velocity	$\leqslant$41.7 km s^{-1}
Single-ion kinetic energy	$\leqslant$9.2 eV
Central energy density	1.5 MJ m^{-2}
Central average power density	30 GW m^{-2}
Heat flux factor	212.1 MWs$^{1/2}$ m^{-2}
Electron density	$\leqslant 2.78 \times 10^{15}$ cm^{-3}
Plasma flux	$\leqslant 1.16 \times 10^{26}$ s^{-1} m^2
Muzzle diameter	2 cm

Table 2. Essential data of QSPA kh-50.

Discharge voltage	$\leqslant$15 kV
Discharge current	$\leqslant$700 kA
Pulse duration	250 μs
External magnetic field	$\leqslant$0.54 T
Plasma stream energy density	0.5…30 MJ m^{-2}
Target heat load	$\leqslant$1.1 MJ m^{-2}
Average heat flux	$\leqslant$4.4 GW m^{-2}
Heat flux factor	$\leqslant$69.6 MWs$^{1/2}$ m^{-2}
Maximal energy of particles	0.2…0.9 keV
Average plasma density	0.2…7 $\times 10^{22}$ m^{-3}
Maximum value of plasma pressure	0.3…1.8 MPa
Plasma stream diameter	$\leqslant$0.18 m

3.2. Plasma thermal shock tungsten target

The process of plasma thermal shock on a tungsten target at different angles is observed. The angles between the plasma and target are 90°, 60°, 30°, and 2°. The experimental phenomena are recorded by a high-speed camera. By observing the thermal shock process, the damage effect of the target at different angles can be analyzed.

As shown in figure 7, the thermal shock process at different angles is captured by a high-speed camera. It can be seen that the plasma reflects in all directions after exposure at 90°. The plasma is reflected along one side after exposure at 30° and 60°. The plasma mainly ablates the edge of the target at

Table 3. Key design parameters and type I ELM characteristic parameters assumed in the analysis [29].

ELM duration	0.5 ms
Divertor ELM energy density	0.2–2 MJ m^{-2}
Heat flux in between ELMs	5–10 MW m^{-2}
Pedestal density	$\sim 8 \times 10^{19}$ m^{-3}
Pedestal temperature	3.5 keV
ELM frequency	1 Hz

2°. The reflection of hydrogen plasma from vessel walls contributes to the recycling of hydrogen and the plasma density in tokamak device [30, 31]. The [25] points out that the reflection coefficient is not only related to the incident energy but also needs to consider the change of angle and surface roughness. However, it is difficult to consider the surface roughness in theoretical calculations. The research group plans to discuss methods of measuring the energy reflection coefficient in the next simulation experiment.

In the full spectrum of the plasma in figure 5, it can be found that the plasma does not emit light at 522 nm–542 nm wavelength under the experimental conditions. In order to observe the thermal shock process more clearly, the author optimized the method with a high-speed camera. When shooting with a high-speed camera, an optical filter is installed in the front of the lens. The optical filter blocks 532 $\pm$ 10 nm of light. The purpose of installing the filter is to prevent the light emitted by the plasma from entering the high-speed camera during the exposure process. The relationship between the transmittance and wavelength of the filter is shown in figure 8. Then, a 532 nm DC continuous wave (CW) laser was used to supplement the light on the target surface in the experiment; the result is shown in figure 9. Figure 9 shows the splashing of droplets or particles on the surface of the target after the thermal shock at 90°. The surface of the target is kept at room temperature before exposure. During multiple exposures, no other means is used to cool the target. In the follow-up experimental scheme, cooling the target will be considered to obtain experimental results more in line with the simulation experiment. It can be seen from figure 9 that the sizes of droplets and particles splashed from the target are of the order

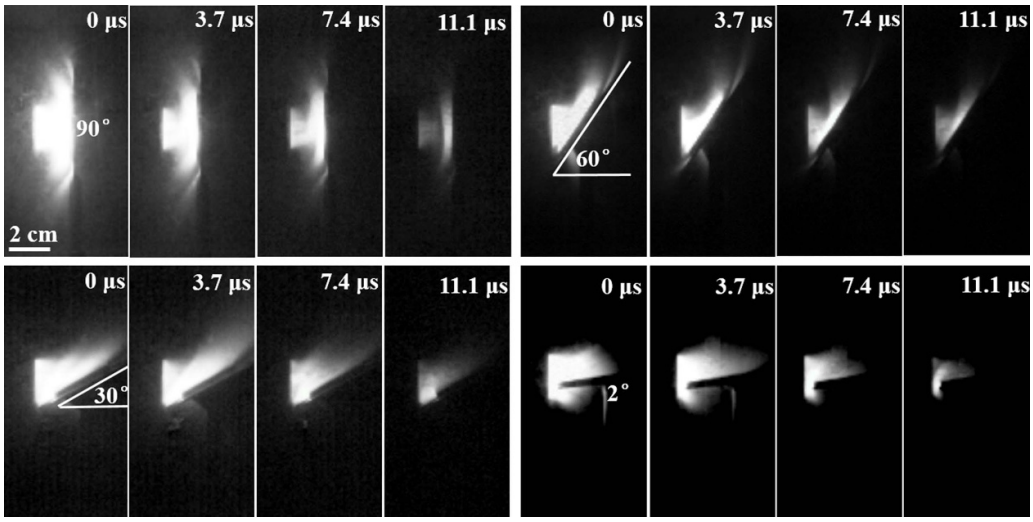

Figure 7. Pictures of the interaction between plasma and tungsten at different angles (90°, 60°, 30°, 2°) under the same discharge parameters using a high-speed camera. The interval time is 3.7 μs and the exposure time is 0.71 μs.

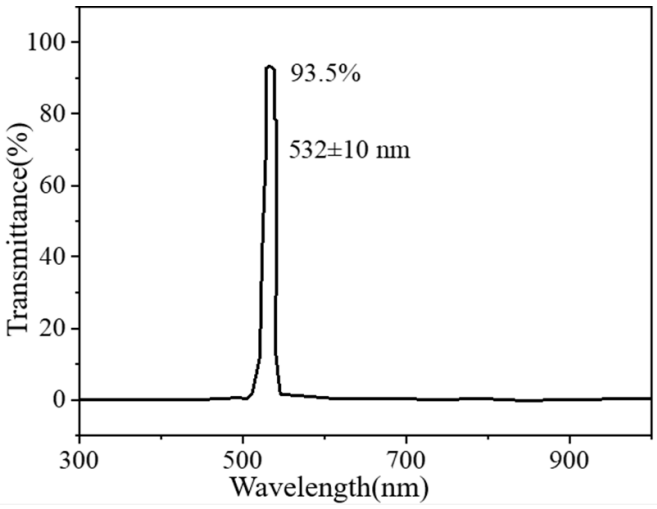

Figure 8. Relationship between transmittance and wavelength of the filter.

of millimeters. Combined with figure 13, there is a liquefaction process on the surface of the target. The muzzle of the gun is 2 cm, and the size of the target is 3 cm × 3 cm. Figure 9 verifies that the plasma thermally diffuses in the process of motion.

In tokamak reactors, tungsten impurities in the plasma can cause large core radiation losses [32]. Generally, the higher the Z, the lower the concentration limit (Z of tungsten is 74). The limit of tungsten concentration in the core is 1×10^{-5}, which shows that even a very small fraction can lead to poor plasma performance up to plasma extinguishing.

Figure 10 shows the sketch of the temporal evolution of the plasma stream and heat flux reaching the target. Thermal diffusion occurs in the transport process of the plasma stream. When the heat flux reaches the target, the energy accumulates on the surface of the target and the surface temperature increases. The rise in temperature results in strong melting of tungsten during the 50 μs pulse and subsequent droplet splashing. The plasma stream is reflected after reaching the target.

3.3. Material characterization

This section studies the damage effect of plasma thermal shocks on the tungsten target. Due to the surface characteristics of the material, ablation, cracks and residual stress are mainly observed. The target size is 30 × 30 × 2 mm, and the surface of the target is polished before the experiment. Figure 13(a) shows the mirror polished surface photographed by a metalloscope. Figure 11 shows the target surface ablation at different angles under 16 kV charge and 20 pulses; (a)–(d) show the surface morphology of the target after plasma thermal shocks at 2°, 30°, 60°, and 90° respectively. It can be seen that the ablation is at the center at 30°, 60° and 90°, and the ablation is mainly at the edge at 2°. There is almost no ablation in the center of the target at 2°. This corresponds to figure 7 above.

As shown in figure 12, with a decrease in the angle, the area of the plasma hitting the target increases, resulting in a decrease in the energy accumulation per unit area. An obvious crack can be seen on the surface of the 90° target after 20 pulses in figure 11. The large temperature difference transformation and the thermal stresses introduced by pulsed plasma loading lead to the generation of the large crack.

The energy distribution of the plasma can be roughly seen from figure 11. At [15], NSC-KIPT shows that a homogeneous distribution of the energy density along the target surface is observed under normal incidence, and the energy density along the target surface is essentially not uniform for inclined plasma irradiation.

The muzzle diameter of the gun is 2 cm and the ablation at the center of the target surface is more serious than that at the edge at the angle of 90°, and the ablation diameter expands to about 3 cm as can be seen in figure 11. This is due to

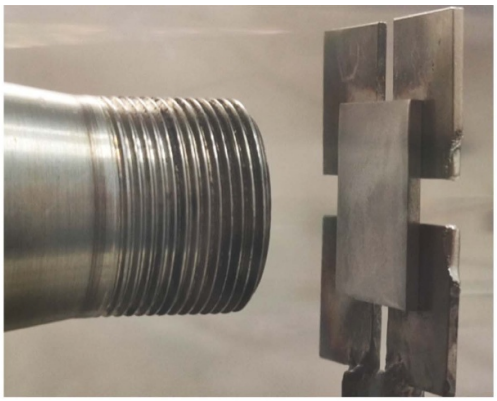

(a)

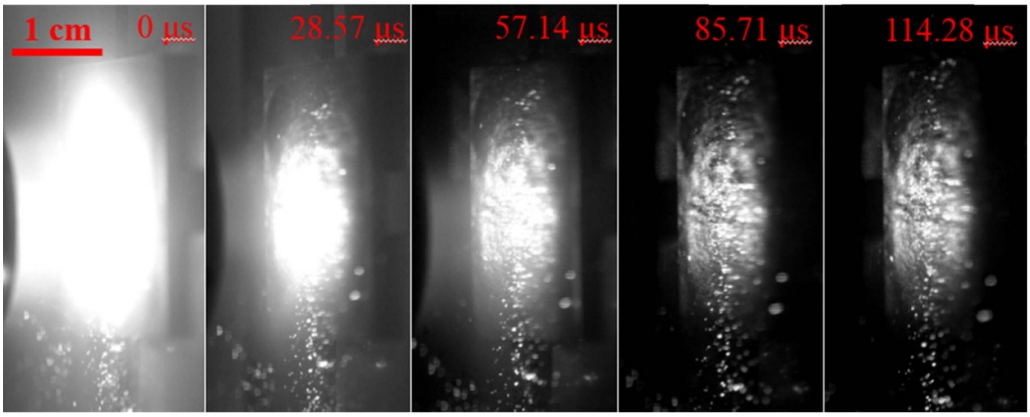

(b)

Figure 9. (a) Actual profile of the sample. (b) Images taken with a high-speed camera. The angle between the surface of the target and the direction of the plasma transport is 90°. A 532 nm laser is used for light compensation. The interval time is 3.7 μs and the exposure time is 2.07 μs.

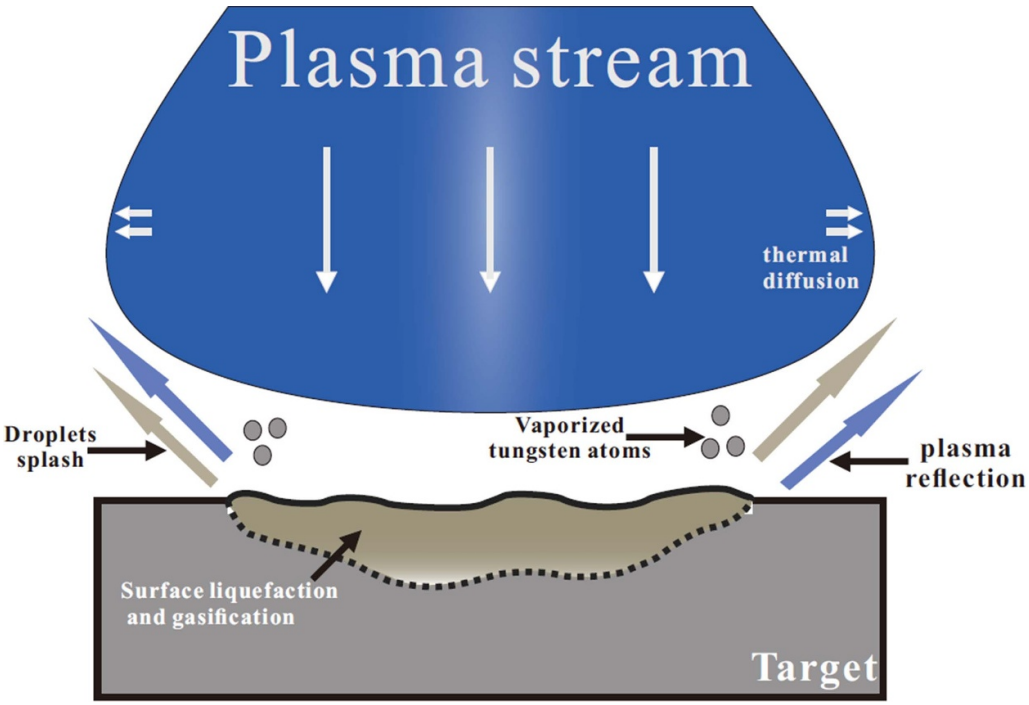

Figure 10. Sketch of the evolution of the plasma stream and heat flux reaching the target.

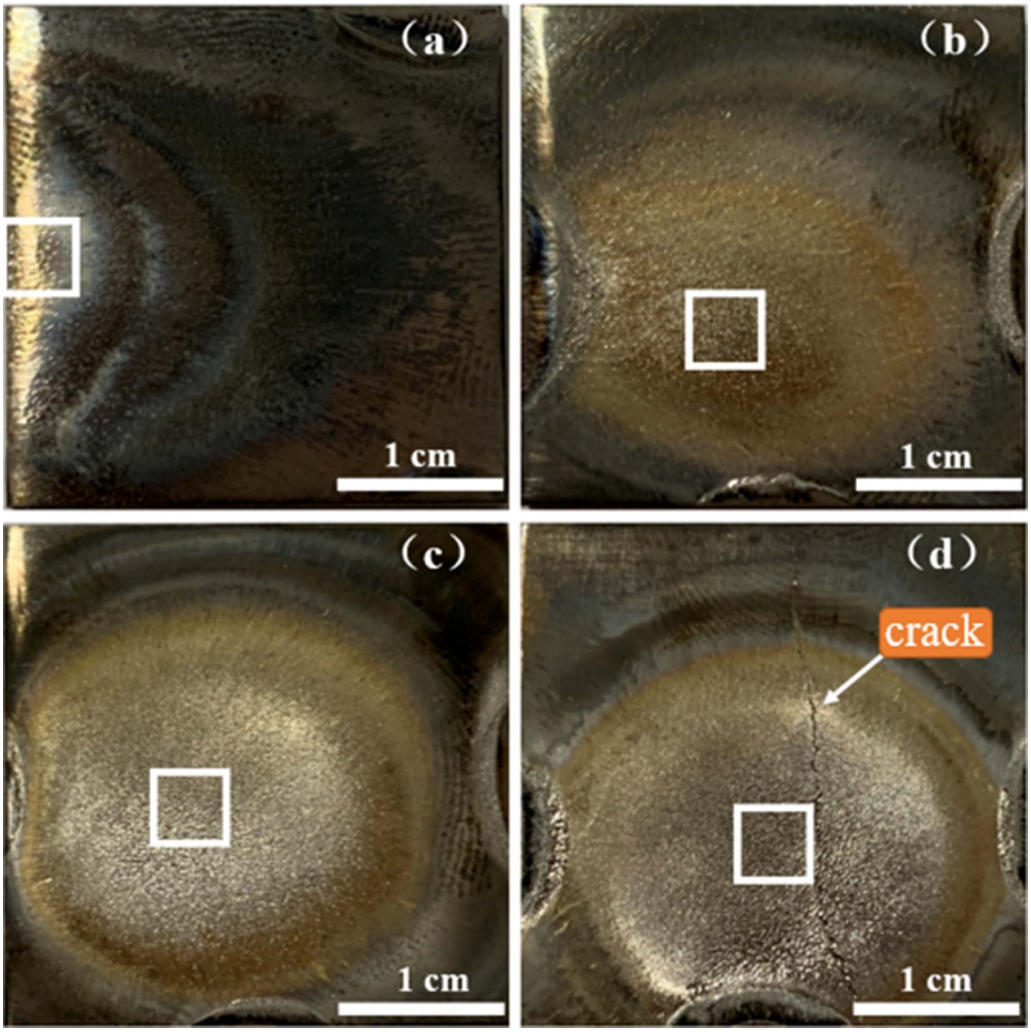

Figure 11. Surface morphology of the target after plasma thermal shock with 20 pulses. The white box is the location for further material characterization. (a) 2°, (b) 30°, (c) 60°, (d) 90°.

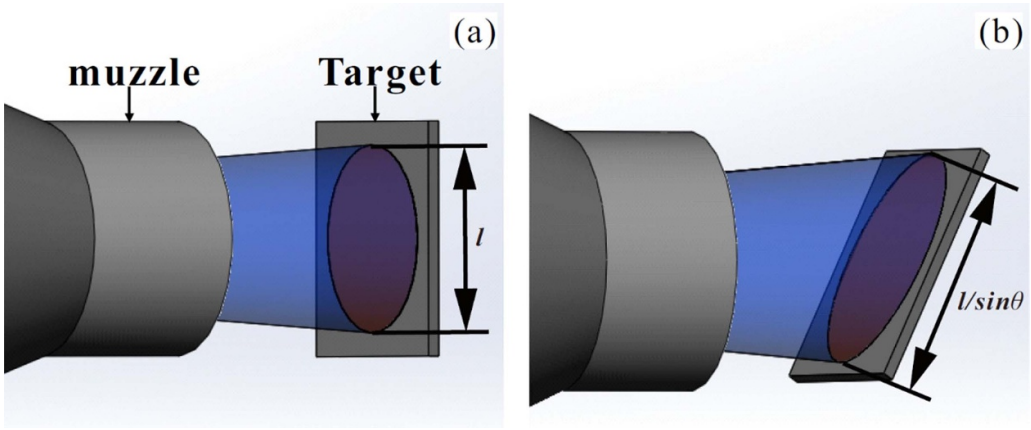

Figure 12. Sketch of the damage area on the surface of the target when the angles are (a) 90° and (b) θ.

the thermal diffusion of the plasma. This corresponds to the energy density discussed in figure 4 above.

The target surface after mirror polishing and the marked positions of the four samples in figure 11 are photographed by a metallographic microscope. The results are shown in figure 13. It can be seen from the photograph that there are obvious traces of liquid flow on the surface of tungsten at 60° and 90° in figures 13(b) and (c). This proves that the surface of the target has begun to melt in the process of the interaction. The melting process of the target surface affects

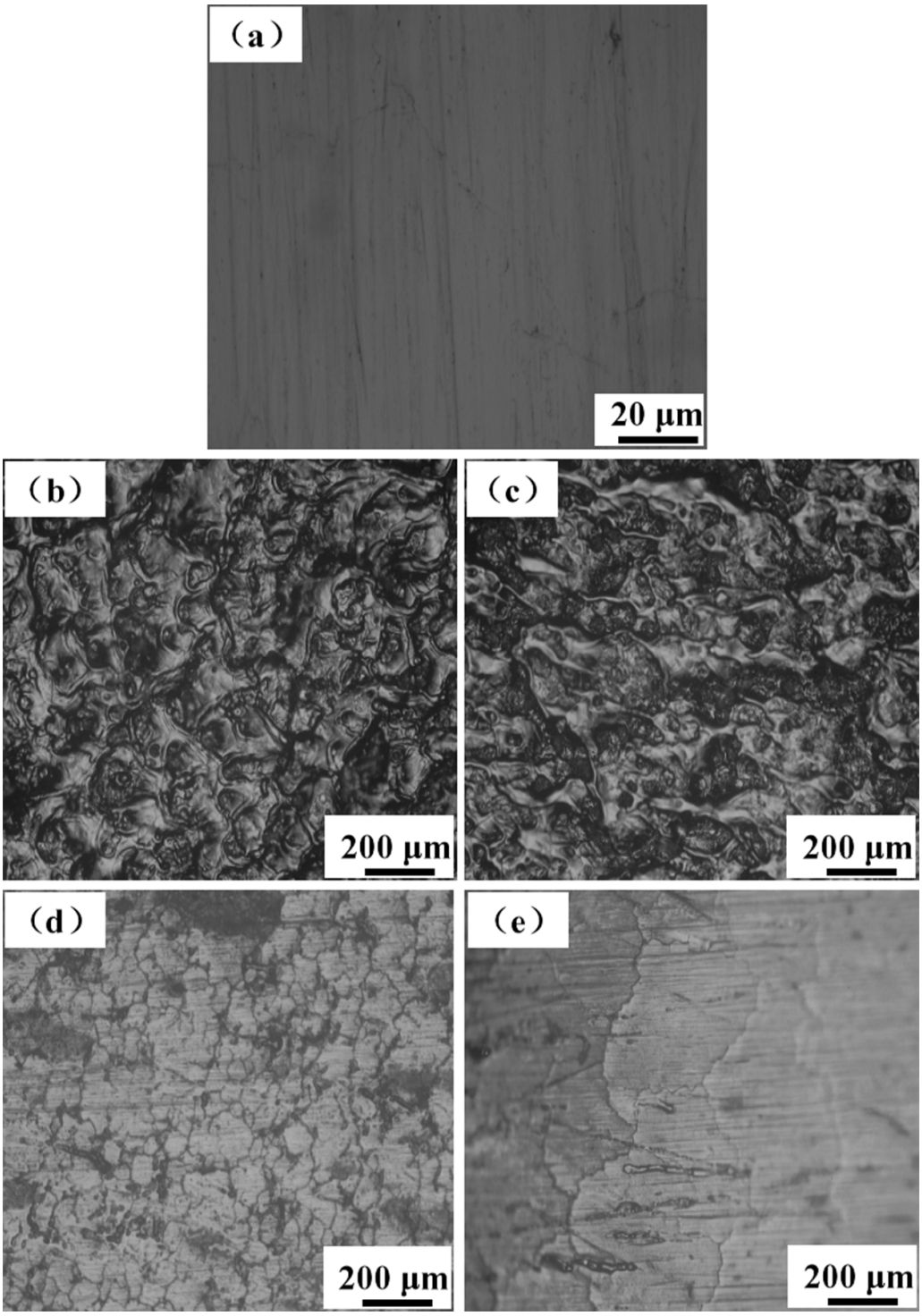

Figure 13. (a) Surface of the target plate after mirror polishing, and (b) 90°, (c) 60°, (d) 30°, (e) 2° is the surface morphology of tungsten target at the mark in figure 11 taken by a metallographic microscope, respectively.

the surface roughness. Combined with the above discussion, the energy accumulated at the surface of the target is high enough to make the surface melt at 60° and 90°. After melting, droplets splash from the surface. Droplet splash and tungsten atom gasification on the surface result in mass loss of the target as shown in table 1. Several dense cracks can be seen on the surfaces of the targets in figure 13. Pulsed plasma loading introduces thermal diffusion, which results in a crack network.

In order to further study the cracks, SEM is needed. It can also be seen that the surface cracks of 2° present a wavy shape in figure 13(e), which is due to the large temperature difference on the surface of the target, and the wavy cracks are produced during the temperature propagation process on the surface.

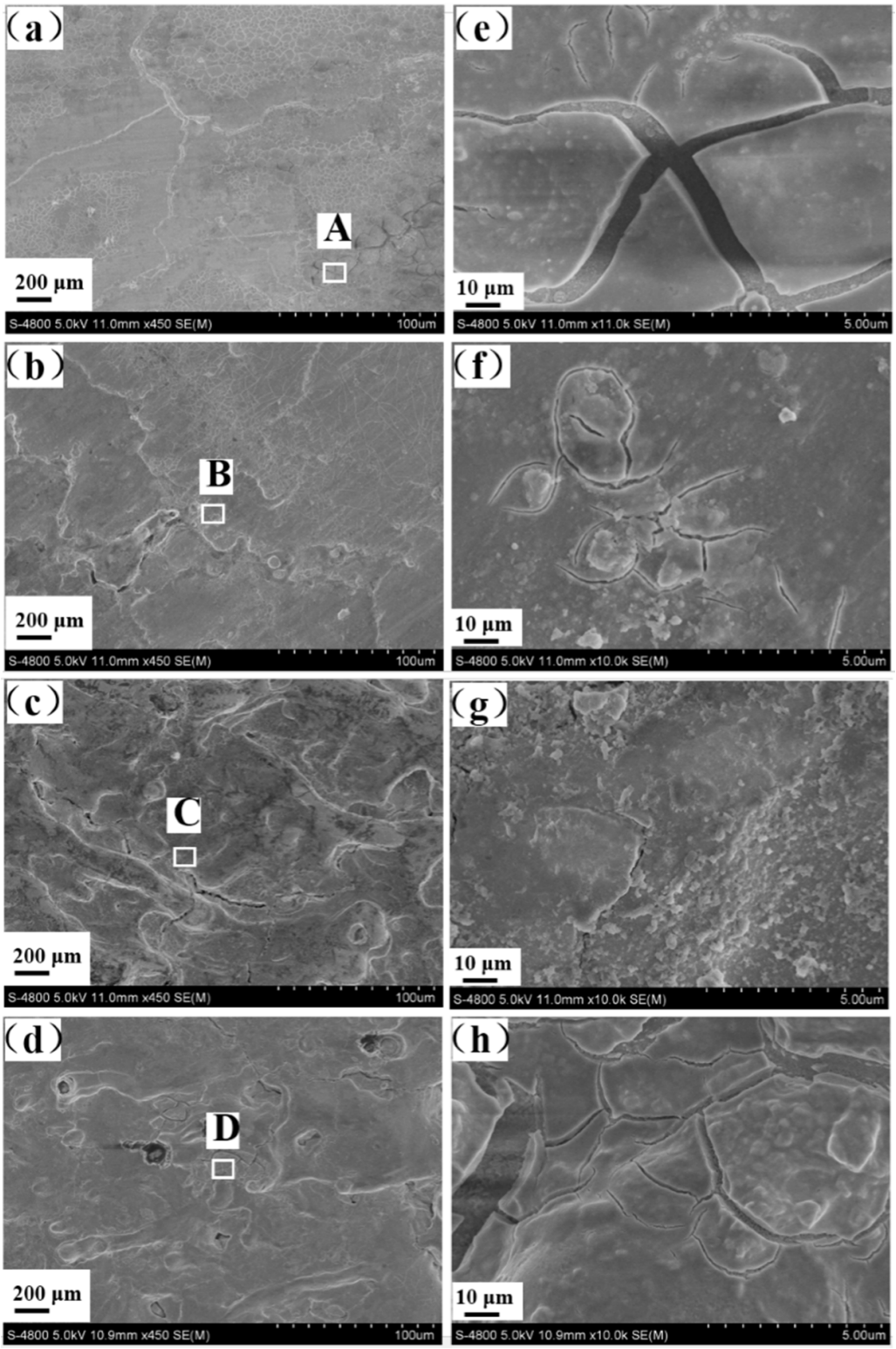

Figure 14. Surface morphology of tungsten target taken by SEM. (a) 2°, (b) 30°, (c) 60° and (d) 90° is the 450 times magnified image at the mark in figure 10, respectively. (e)–(h) is the 11 K times magnified image at the marked positions (A), (B), (C), and (D), respectively.

Figure 14 shows the target surface photographed by scanning electron microscopy (SEM), in which the edge is photographed at 2° and the center is photographed at 30°, 60°, and 90°. The shooting positions in (a)–(d) are the marked positions of the samples in figure 11. It can be seen from (c) and (d) that when the included angle is 60° and 90°, the target surface is severely ablated. The areas (A), (B), (C) and (D) in the figure are enlarged 11 K times by SEM to obtain (e)–(h).

In figures 14(e) and (f), it can be found that there are obvious cracks on the surface of the target when the angle is

Table 4. Mass and mass loss of the tungsten target before and after 20 pulses.

Degree (°)	Before (g)	After (g)	△ (g)
2	29.10	29.09	0.01
30	29.49	29.47	0.02
60	28.49	28.46	0.03
90	27.87	27.84	0.03

Table 5. Surface residual stress at the mirror polished surface at different angles after 20 pulses.

Angle	Mirror surface	2°	30°	60°	90°
Residual stress (MPa)	-892.1 ± 14.2	286 ± 14.4	302 ± 13.5	322 ± 12.6	294 ± 6.3

2° and 30°. From figures 14(g) and (h), it can be found that the target surfaces with the angles of 60° and 90° are uneven, and fine cracks with a network are found on the resolidified surface of the shedding area. This may be due to the target surface falling off during the plasma thermal shocks at 60° and 90°, resulting in the uneven target surface. In the process of thermal shock, the temperature difference between the target surface and a certain depth causes cracks on the target surface.

Combined with figures 11–14, it can be found that the damage effect on the target decreases with a decrease in the angle. In the above calculation, the maximum kinetic energy of hydrogen ion is 9.2 eV, which is far less than the sputtering threshold of tungsten. The damage effect of plasma on the target is mainly due to the increase in surface temperature caused by the energy accumulation on the surface. The sudden cooling and heating of the target surface makes the tungsten material brittle [1, 10, 14], and the large surface temperature gradient produces uneven expansion deformation. The surface cracks are formed in the process of the damage effect.

Referring to the previous report, in order to further analyze the damage effect of tungsten target in the simulation experiment, the research team analyzed the mass loss of target plate after bombardment at different angles. Table 4 shows the mass and mass loss of the target before and after 20 pulses. The mass loss of the target is mainly due to the droplet splash and tungsten atom gasification, and may also be caused by liquefaction or other damage effects. In this simulation experiment, it is found that there will be a certain amount of tungsten impurity sputtering without external magnetic field constraint, which will seriously affect the stable operation of the tokamak device combined with the discussion above.

In order to further verify the generation mechanism of the surface crack of the target, the macroscopic residual stress of the target after thermal shock is measured by XRD. The average first kind of internal stress at the marked position on the target surface in figure 11 is measured in this paper.

Table 5 shows the measured surface residual stress at the mirror polished surface, the edge of the 2° and the center of the 30°, 60° and 90° after 20 pulses. It can be seen from table 5 that the residual stress of the original mirror polished surface is -892.1 ± 14.2 MPa. The material of the tungsten target is fabricated by longitudinal stretching and transverse hammering, so the surface residual stress of the original mirror is negative. The surface residual stresses of 2°, 30°, 60° and 90° are 286 ± 14.4, 302 ± 13.5, 322 ± 12.6 and 294 ± 6.3 respectively. It can be found from table 5 that the residual stress on the surface of the target after thermal shock increases, from compressive stress to tensile stress. In the process of plasma thermal shock on the target, the temperature of the target surface rises rapidly, forming a large temperature gradient, resulting in uneven expansion deformation and resulting in residual stress on the surface. When the angle between the plasma transport direction and the target is 2°, 30° or 60°, the surface stress increases with an increase in the angle. With an increase in the angle, the accumulated energy of plasma on the surface of target increases and the temperature gradient of the target falls, so the surface residual stress increases. As can be seen in figure 11(d) above, under the condition of 90°, there is an obvious crack after 20 pulses. The large crack releases the stress on the surface of the target so the measured residual stress decreases slightly.

4. Conclusion

In this paper, the damage effect of ELM-I on a divertor target in a tokamak under H-mode is simulated by thermal shocks of pulsed plasma on a tungsten target. A discharge system of a tapered coaxial accelerator is set up. The conclusions are as follows:

The plasma is produced by a charging voltage of 16 kV and pre-filled mode discharge, and the working gas is hydrogen. The current waveform is a gradually decreasing sine wave, and there are always multiple current paths in the coaxial gun during the discharge process. During the transport of the plasma, thermal diffusion causes the energy density to decrease from the center to the edge. The duration of the plasma stream is about 50 μs. The heat flux factor is 212.1 $\mathrm{MWs}^{1/2}\ \mathrm{m}^{-2}$. In the next step, it is necessary to change the power supply and circuit to increase the duration and reduce the heat flux factor below 100 $\mathrm{MWs}^{1/2}\ \mathrm{m}^{-2}$. It is also necessary to shorten the pulse period and cool the target during the discharge process.

The damage effect is at the center at 30°, 60° and 90°, and there is almost no ablation in the center of the target at 2°. In the 90° exposure process, it can also be observed that there are millimeter-sized droplets or particles splashing from the surface of the target.

Based on the actual situation of tokamak devices, this paper makes an in-depth analysis of the material characterization (surface liquid splash, mass loss, etc) after bombardment at different angles, which is different from previous reports. The diagnosis method is introduced in detail. There are obvious traces of liquid flow on the surface at 60° and 90°, and the surface is uneven, which indicates that the target surface liquefies during the interaction. Small cracks are found on the uneven surface. The melting process contributes considerably to the surface roughness. There are obvious cracks of the order of micrometers on the surface. The mass loss of the target is mainly due to the droplet splash and tungsten atom gasification, and may also be caused by liquefaction or other damage effects.

With the decrease in angle, the accumulated energy of the surface decreases, so the stress decreases. At the angle of 90°, an obvious crack appears on the surface of the target plate, which releases the stress, and reduces the surface residual stress.

Data availability statement

All data that support the findings of this study are included within the article (and any supplementary files).

Acknowledgment

This work is supported by National Key R&D Program of China (Grant No. 2017YFE0301206).

ORCID iDs

Chongxiao Zhao https://orcid.org/0000-0003-3899-9924
Qikun Pan https://orcid.org/0000-0002-6386-6747
Liang Yang https://orcid.org/0000-0003-0239-0666
Dezhen Wang https://orcid.org/0000-0003-0517-7318

References

[1] Tereshin V I, Bandura A N, Byrka O V, Chebotarev V V, Garkusha I E, Landman I, Makhlaj V A, Neklyudov I M, Solyakov D G and Tsarenko A V 2007 Application of powerful quasi-steady-state plasma accelerators for simulation of ITER transient heat loads on divertor surfaces *Plasma Phys. Control. Fusion* **49** A231–9
[2] Dojinovi I P 2010 Plasma flow interaction with ITER divertor related surfaces *J. Phys.: Conf.* **257** 012033
[3] Kikuchi Y, Nakanishi R, Nakatsuka M, Fukumoto N and Nagata M 2010 *IEEE Trans. Plasma Sci.* **38** 232–6
[4] Kikuchi Y *et al* 2011 *J. Nucl. Mater.* **415** S55–8
[5] Philipps V 2011 *J. Nucl. Mater.* **415** S2–9
[6] Sakuma I, Kikuchi Y, Kitagawa Y, Asai Y, Onishi K, Fukumoto N and Nagata M 2015 *J. Nucl. Mater.* **463** 233–6
[7] Arkhipov N I, Bakhtin V P, Kurkin S M, Safronov V M, Toporkov D A, Vasenin S G, Zhitlukhin A M and Würz H 2000 Material erosion and erosion products in disruption simulation experiments at the MK-200 UG facility *Fusion Eng. Des.* **49–50** 151–6
[8] Case A, Messer S, Bomgardner R and Witherspoon F D 2010 *Phys. Plasmas* **17** 053503
[9] Yang L, Zhang J L, Yan H J, Hua Y and Ren C S 2017 *Acta Phys. Sin.* **66** 055203
[10] Bakaeva A, Makhlai V, Terentyev D, Zinovev A, Herashchenko S and Dubinko A 2019 *J. Nucl. Mater.* **520** 185–92
[11] Arkhipov N I, Bakhtin V P, Kurkin S M, Safronov V M, Toporkov D A, Vasenin S G, Wuerz H and Zhitlukhin A M 1996 Study of structure and dynamics of shielding layer for inclined incidence of plasma stream at MK-200 facility *J. Nucl. Mater.* **233–237** 767–70
[12] Zhao C, Song J, Qi L, Ma C, Hu J, Bai X and Wang D 2020 *Fusion Eng. Des.* **158** 111870
[13] Zhang J L, Yang L, Yan H J, Hua Y and Ren C S 2015 *Acta Phys. Sin.* **64** 7
[14] Mao R, Fedorczak N, Ciraolo G, Bufferand H, Marandet Y, Bucalossi J, Tamain P, Serre E, Zheng G Y and Li J X 2019 Impact of an alternative divertor configuration on plasma detachment: pure deuterium simulations using the SOLEDGE2D-EIRENE edge transport code for HL-2M scenarios *Nucl. Fusion* **59** 106019
[15] Garkusha I E *et al* 2019 Influence of a magnetic field on plasma energy transfer to material surfaces in edge-localized mode simulation experiments with QSPA-M *Nucl. Fusion* **59** 086023
[16] Cassibry J T, Thio Y C F and Wu S T 2006 *Phys. Plasmas* **13** 053101
[17] Liang Y, Yan H, Zhang J, Hua Y and Ren C 2014 Characteristics of coaxial gun pulse discharge plasma and its axial velocity analysis *Gaodianya Jishu/High Volt. Eng.* **40** 2113–8
[18] Qi L, Zhao Z, Yan H, Wang T and Ren C 2019 *Acta Phys. Sin.* **68** 3
[19] Matsumoto T *et al* 2016 *Rev. Sci. Instrum.* **87** 053512
[20] Woodall D M and Len L K 1985 *J. Appl. Phys.* **57** 961–4
[21] Poehlmann F 2010 Investigation of a plasma deflagration gun and magnetohydrodynamic Rankine-Hugoniot model to support a unifying theory for electromagnetic plasma guns *Doctoral Dissertation* Stanford University
[22] Liu S, Huang Y, Guo H, Lin T, Huang D and Yang L 2018 *Phys. Plasmas* **25** 053506
[23] Liu S 2019 Study on the electromagnetically riven plasma characteristics of a parallel-rail accelerator *Acta. Phys. Sin.* **67** 065201
[24] Ueda Y, Schmid K, Balden M, Coenen J W, Loewenhoff T and Ito A 2017 *Nucl. Fusion* **57** 092006
[25] Witherspoon F D, Case A, Messer S J, Bomgardner II R, Phillips M W, Brockington S and Elton R 2009 *Rev. Sci. Instrum.* **80** 083506
[26] Rieker G B, Poehlmann F R and Cappelli M A 2013 *Phys. Plasmas* **20** 73115
[27] Liu S, Huang Y, Zhang Y, Zhan W, Yu M and Yang L 2018 Optical emission spectroscopy investigation of the current sheet in a small-bore parallel-plate electromagnetic plasma accelerator *J. Plasma Phys.* **25** 113505
[28] Zhao C, Laingwen Q, Yan H, Wang T and Ren C 2019 *Acta Phys. Sin.* **68** 10

[29] Federici G, Loarte A and Strohmayer G 2003 Assessment of erosion of the ITER divertor targets during type I ELMs *Plasma Phys. Control. Fusion* **45** 1523
[30] Chang M, Sang C, Sun Z, Hu W and Wang D 2018 The effects of particle recycling on the divertor plasma: a particle-in-cell with Monte Carlo collision simulation *Phys. Plasmas* **25** 052507
[31] Lunt T, Reimold F, Wolfrum E, Carralero D, Feng Y and Schmid K 2017 Influence of the first wall material on the particle fuelling in ASDEX Upgrade *Plasma Phys. Control. Fusion* **59** 055016
[32] Chebotarev V V, Garkusha I E, Garkusha V V, Makhlaj V A, Mitina N I, Solyakov D G, Tereshin V I, Trubchaninov S A, Tsarenko A V and Wuerz H 1996 Characteristics of transient plasma layers produced by irradiation of graphite targets by high power quasi-stationary plasma streams under the disruption simulation conditions *J. Nucl. Mater.* **233** 736–40